

Enhanced Anti-Microbial Activity in Green Concrete Specimens Containing Fly Ash, Nanophase Modifiers, and Corrosion Inhibitor

Manu Harilal,^{a,b} Sudha Uthaman,^c R.P. George ,^a B. Anandkumar,^a C. Thinaharan,^a John Philip,^{a,b} and U. Kamachi Mudali^d

^aCorrosion Science and Technology Division, IGCAR, Kalpakkam, India; rpg1961@gmail.com (for correspondence)

^bHomi Bhabha National Institute, Mumbai, India

^cCentre for Nanoscience and Nanotechnology, Sathyabama Institute of Science & Technology, Chennai, India

^dHeavy Water Board, Mumbai, India

Published online 00 Month 2018 in Wiley Online Library (wileyonlinelibrary.com). DOI 10.1002/ep.13102

This study reports the anti-bacterial properties of green concrete containing fly ash, nanoparticle modifiers, and a corrosion inhibitor. Four different concrete specimens, namely control concrete containing ordinary portland cement (CC), fly ash concrete containing 40 wt % fly ash (CF), modified fly ash concrete containing nano-TiO₂ and nano-CaCO₃ (1 wt % each) called CFN, and CFN with 2 wt % corrosion inhibitor (CFNI) are used in the present study. Among the four specimens exposed to microbial culture, CFNI showed minimal bacterial attachment and biofilm density, which is further corroborated from Epifluorescence microscopy and 3D confocal laser scanning microscopy. The CFNI specimens showed the least pH reduction among the four, which resulted in the enhanced microbial resistance. The results unambiguously confirm the synergetic effects of nanophase modifiers and NaNO₂ based inhibitor in controlling microbial activity in concrete specimens. The results have promising applications in formulating concrete structures that are exposed to harsh environmental conditions. © 2018 American Institute of Chemical Engineers Environ Prog, 2018

Keywords: green concrete, nanoparticles, corrosion, anti-bacterial, confocal laser scanning microscopy

INTRODUCTION

Nuclear structures are generally designed with a service life of about 40 years. The present interest is to extend their life span over 60–100 years, using the new technologies, in order to reduce the cost per unit power production. There are many concrete structures associated with a power plant, for example, cooling water system, intake pipes, etc., which are exposed to harsh and aggressive marine environments, either directly or indirectly. The structural stability of concrete structures in contact with seawater is of extreme importance for the long term service of a nuclear industry [1–3]. Concrete structures are severely affected by factors like carbonation, ingress of chloride and sulfate ions, microbial corrosion, etc. The corrosion due to acid producing microbes takes place

through the formation of active biofilms on the concrete surface [4]. Among various factors affecting the deterioration of concrete structures, the one due to biological origin is very significant in aggressive environments due to the production of biogenic corrosive substances by the microorganisms [5,6]. Microorganisms form colonies over the surface of concrete and results in the structural, functional, and aesthetic damage of concrete structures [7]. Microbial growth over concrete surfaces can take place under a wide range of environments like elevated humidity, prolonged freezing and thawing, high levels of carbon dioxide or chloride ingress, high concentrations of sulfates, and very small amount of acids [8].

The scope of improving the durability and performance of concrete through incorporation of mineral and chemical admixtures paved the way to development of a class of concrete called high performance concrete (HPC) with a reduced water to cement (w/c) ratio and enhanced properties. There are many pozzolanic materials like burning rice husk, blast furnace slag, fly ash, etc. that can replace cement in the production of concrete. But CO₂ emissions from burning rice husk also form a part of the global carbon cycle [9]. Thus, the need of the hour is to reduce the emission of CO₂ in the construction industry through the application of sustainable techniques and technologies [10]. Among the most commonly used mineral admixtures, fly ash, a waste product from coal based power plants, is incorporated in concrete in order to reduce the utilization of cement and to improve its durability, thereby making it an environment friendly green concrete. Despite these advantages, there are some early-age performance issues reported for fly ash concrete like low early-age strength, high calcium leaching, etc. [11,12].

Studies show that nanoparticles can improve the cement hydration process and density the microstructure. It was reported that the incorporation of nano-CaCO₃ stimulates the hydration of cement and helps in the attainment of modulus of elasticity during the early stage. It has also been found that the reduction in pH on the surface of concrete specimens incorporated with nano-TiO₂ is minimal and, therefore, increases the anti-bacterial resistance of the concrete [13,14]. A comprehensive study by Sudha *et al.* [15] has shown that incorporation of

nanoparticles of CaCO₃ and TiO₂ in 1:1 proportion can greatly enhance the properties of fly ash concrete.

Studies also show that addition of corrosion inhibiting admixture to concrete can highly improve the resistance of reinforcing steel against deterioration in aggressive and harsh environments [16]. Among the commonly available methods for the prevention of reinforcement corrosion, use of corrosion inhibiting admixtures is found to be attractive. Nitrite based inhibitors are considered to be the most effective, as nitrite acts as a passivator due to its excellent oxidizing capabilities [17]. The rate of formation of the passive film due to nitrites is very swift and thus nitrite shows good performance among the several available corrosion inhibitors [18]. Further, Montes *et al.* [19] had demonstrated the individual effect of fly ash and inhibitor addition in enhancing the corrosion resistance of reinforcements and also the synergistic effect of the two.

In this study, an attempt was made to improve the antibacterial properties of nanophase modified fly ash concrete by adding a corrosion inhibitor. Detailed investigations were carried out to evaluate the synergy between fly ash, nanoparticles, and corrosion inhibiting admixture in imparting microbial resistance to HPC. To evaluate the anti-bacterial characteristics of HPC, exposure studies were done in two different aggressive microbial cultures—Mixed Aerobic Bacterial (MAB) culture and anaerobic Sulfate Reducing Bacterial (SRB) culture. The four different compositions of concrete are prepared and are designated as CC, CF, CFN, and CFNI (Table 1).

EXPERIMENTAL PROGRAM

Mix Design and Proportioning

The mix proportion for HPC was designed based on the recommendations given in IS 10262:2009. Four different mixes of mortar specimens of M45 grade were prepared and designated as control concrete (CC) with 100% Ordinary Portland Cement (OPC), CC partially replaced with 40 wt % fly ash called fly ash concrete (CF), CF incorporated with 1 wt % TiO₂ and 1 wt % CaCO₃ nanoparticles designated as CFN and CFN admixed with 2 wt % sodium nitrite based corrosion inhibitor designated as CFNI. The detailed mix design used for casting the specimens is given in Table 1.

Materials

OPC 43 grade (PENNA) with a specific gravity of 3.12 and a fineness module of 5.0 conforming to IS 8112-2013 was used for casting the mortar specimens. Class F fly ash (Siliceous type) procured from Ennore Thermal Power Plant, Chennai conforming to IS 3812:1981 was used as the cement replacement material. Crushed black granite with a maximum size of 20 mm and 12 mm were used in equal proportions as the coarse aggregates. Crushed gravel with a maximum size of 4.75 mm and specific gravity of 2.83 was used as the fine aggregates. The selection of aggregates was according to IS 383:1970 standards. RheoBuild 1125, a sulphonated naphthalene based high range water reducing admixture was used in this study as the superplasticizer conforming to ASTM C494 type F [20]. Corrosion inhibitor used in this study is sodium nitrite based anodic mixed inhibitor solution which is commercially available and dark brown in color. The pH and density

of the inhibitor solution was 11.10 and 1.06 g/cc, respectively. The laboratory grade nano-titania and nano-calcium carbonate were purchased from Merck, Germany with an initial particle size of 400–500 nm. It was subjected to ball milling to reduce its size in the range of 100–120 nm.

Preparation of Cylindrical Mortar Specimens

Cylindrical mortar specimens of 90 mm diameter and 10 mm thickness were cast using molds in the form of petri plates and cured for 28 days in fresh water in laboratory atmosphere. After curing, the mortar specimens were polished with 80 grit silicon carbide polishing paper to make the surface even. These specimens were then exposed in triplicate in the two microbial cultures and withdrawn after the exposure period of 7 days.

Preparation of Microbial Culture Media

Different types of bacterial species (aerobic and anaerobic) have different mode of action on the material [21]. In order to test the antibacterial property of mortar specimens, the specimens were exposed to a mixture of both aerobic and anaerobic bacterial culture.

MAB Culture Media

A group of mixed bacterial colonies (two gram-negative rod shaped and one gram-positive cocci shaped) were isolated from the surface of concrete specimens exposed to sea water. The isolated bacterial colonies were inoculated into the sterilized 10% nutrient broth (Peptic digest animal tissue 5 g/L, NaCl 5 g/L, beef extract 1.50 g/L, distilled water 1 L, and pH 7.4 ± 0.2) and incubated at 37°C for 24 h.

After 24 h, 1 mL of bacterial culture was inoculated into a sterilized acrylic jar containing 1000 mL of 10% nutrient broth and incubated at the same conditions mentioned above. The extent of microbial growth was then confirmed by staining the culture using acridine orange (AO). A drop of bacterial culture media was placed on a well cleaned microscopic slide and air dried for few minutes. Then the slide was stained with 0.1% AO solution for 15 min and washed thereafter. The slide was visualized under an epifluorescence microscope (Nikon Eclipse E600) for identifying the presence of active cells over the surface. The exposure media was replaced daily with 800 mL of fresh 10% nutrient broth to keep the bacterial cells alive. The mortar specimens of all the four mixes were exposed in the prepared culture media in triplicate.

SRB Culture Media

The surface of the concrete specimens exposed in seawater for a period of 1 year was scraped to collect the biofilm attached over the surface. This biofilm was inoculated into a specific growth medium of sulfate reducing bacteria (SRB) known by the name Postgate medium (casein enzyme hydrolysate 6 g/L, sodium sulfate 0.6 g/L, sodium sulfite 0.6 g/L, ferric citrate 0.06 g/L, sodium chloride 5 g/L, and pH 7.1) [22]. Since SRB is an anaerobic bacterium, the favorable condition for its growth was provided by arresting the oxygen supply using a parafilm tape. The medium was incubated at 37°C for 24 h and further inoculated to 1000 mL of Postgate medium in an acrylic jar. The growth of SRB in the prepared culture

Table 1. Mix proportions of four types of specimens.

Type of specimen	Cement (kg/m ³)	Fly ash (kg/m ³)	F.A (kg/m ³)	TiO ₂ (kg/m ³)	CaCO ₃ (kg/m ³)	Inhibitor (kg/m ³)
CC	450	–	797	–	–	–
CF	270	180	744	–	–	–
CFN	261	180	733	4.5	4.5	–
CFNI	252	180	724	4.5	4.5	9.0

medium was confirmed as mentioned in the previous section. The fresh nutrient medium was added daily to maintain the growth of bacteria in the biofilm over the surface of concrete specimens. The medium was changed inside a biosafety cabinet. Another set of polished mortar specimens were exposed in this medium in triplicate.

The 24 h incubated 10% nutrient broth culture of MAB and Postgate medium of SRB were kept in laboratory conditions with an air conditioned environment maintained at 28°C–29°C. Hence, there was no effect of temperature on the culture media. Further, light and CO₂ had no effect on the growth of MAB and SRB culture media. For MAB culture, the presence of O₂ is required to maintain the aerobic environment and this is accomplished through the cotton plugged over the lid. However, for SRB culture, the addition of sodium sulfite in the media scavenges the O₂ in the air cover over the media inside the container. Daily replenishment of the medium ensured the scavenging of O₂ to maintain the anaerobic conditions.

Post Exposure Analysis

Degradation Studies

The photographs of the mortar specimens exposed in bacterial cultures were captured using a Samsung Galaxy DSLR camera (D3 Nikon Make) to get a qualitative idea on the morphology of the surface after exposure in bacterial culture. In order to measure bulk pH, the mortar specimens were crushed using a manually operated mallet and then finely ground by using a mortar and pestle. About 5 g of this powder was then mixed with 100 mL of Millipore water (14.3 MΩcm resistivity) and then stirred using a magnetic stirrer (REMI 1MLH, India). The pH of the mortar specimens was then measured using an ecoTestr pH 1 pH tester (Singapore). The quantitative reduction in pH before and after exposure was measured and recorded. The different parameters like thickness and diameter of the specimens were measured using a digital Vernier caliper (Mitutoyo Digimatic, Japan) before and after exposure in the microbial culture. Similarly, the weight of the mortar specimens was also measured using a digital weighing balance (AND, GH-252). The differences in the dimensional parameters and loss in weight were calculated under both the exposure conditions and tabulated. Three sets of specimens were used for the exposure studies and the standard deviation of the parameters is reported. Figure 1 shows the exposed specimens in acrylic jars containing culture mediums.

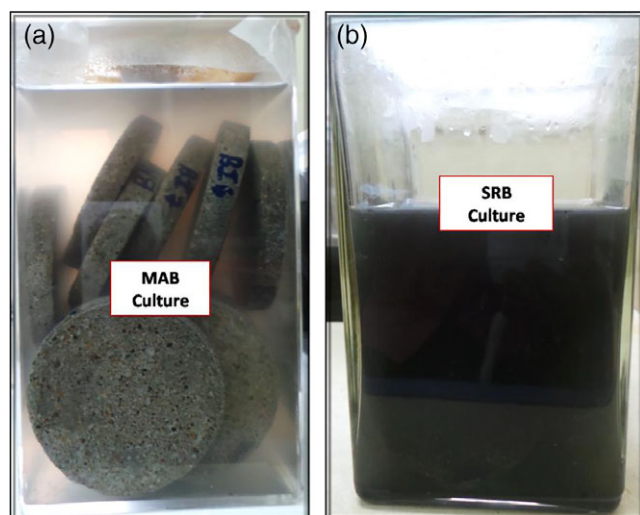


Figure 1. CC, CF, CFN, and CFNI Mortar specimens exposed in (a) MAB culture and (b) SRB culture. [Color figure can be viewed at wileyonlinelibrary.com]

Biofilm Characterization Studies

The total bacterial density is calculated by the determination of total viable count (TVC) [3] using culture techniques in nutrient agar. The biofilm attached on the surface of mortar specimens exposed in both the culture media were scraped using a sterile brush and mixed with phosphate buffer solution (KH₂PO₄ 0.0425 g/L and MgCl₂ 0.19 g/L) and was used for further analysis. The homogenized suspension containing phosphate buffer and biofilm was serially diluted and plated as per pour plate method using nutrient agar as the bacterial growth medium. The plates were incubated for 24 h at 37°C and the bacterial density was determined as per APHA standards [23]. TVC was calculated by estimating the number of colony forming units (CFU) per square centimeter of the sample and then tabulated. The estimation of biochemical composition of the biofilm like carbohydrate and protein gives quantitative information on the content of organic materials in the biofilm scraped from the surfaces of the specimens [3]. The amount of carbohydrate and protein in the biofilms was estimated by Anthrone [24,25] and Lowry's method [26], respectively.

Epifluorescence Microscopic Studies

The mortar specimens exposed in both the microbial cultures were observed under an Epifluorescence Microscope (Nikon Eclipse E600) to characterize the biofilms that are formed on the surface. All the specimens were stained with 0.1% AO solution and then rinsed with Millipore water after a time period of 30 min to remove excess stains. AO is a fluorescent dye used to differentiate between DNA and RNA. The presence of green fluorescence with a wavelength of the order of about 525 nm indicates AO intercalation with DNA of the bacterial cells. However, AO intercalates with RNA of an actively metabolizing bacterial cell and then give orange fluorescence at a wavelength greater than 630 nm [27,28]. On mortar surfaces, AO was also found to fluoresce green due to the presence of oxides in the absence of biofilm [29].

Confocal Laser Scanning Microscope Studies

Lawrence *et al.* has reported that confocal laser scanning microscope (CLSM) is the most versatile and productive non-destructive technique in the characterization of biofilms [30]. Mortar specimens exposed in bacterial cultures were stained with DNA-binding fluorochrome 4',6-diamidino-2-phenylindole (DAPI) to visualize the total cells adhered to the surface. When excited with a suitable source, DAPI fluoresces in the blue to cyan range at 461 nm. The specimens were fixed with formalin (3.7% final concentration) and subsequently stained with DAPI (1.0 mg/mL) for 15 min as described elsewhere [31,32]. The stained specimens were visualized under LSM880 Confocal Microscope (Carl Zeiss, Germany) and the biofilm images were recorded using Zen 2.0 software. The specimens were irradiated using an Argon laser (excitation and emission range of 400 and 410–500 nm respectively) at an excitation wavelength of 405 nm.

Tile scans, 3D, and orthographic views of biofilms were reconstructed with LSM Image Browser (Carl Zeiss Microscopy GmbH, Munich, Germany) to analyze the biofilm thickness over the specimen surface at micro-scale based on the CLSM image stacks. Digital image analysis of the CLSM images was used to determine the depth of biofilm formation over the surface [33,34]. Image analyzer J V1.45 and COMSTAT 2 software were used to quantify the micro-scale biofilm structure. Parameters including biovolume, mean thickness, maximum thickness, roughness coefficient, surface to volume ratio, and the average diffusion distance were analyzed using COMSTAT 2 software as described elsewhere [35,36].

X-Ray Diffraction Studies

The mortar specimens exposed in the cultures were broken into small pieces with the help of a mallet. These particles

were then crushed and made into very fine powder. The various phases present in the different mixes of mortar specimens were then analyzed by powder X-ray diffraction method. The XRD analysis was done using a X-ray diffractometer (Inel-EQUINOX 2000 diffractometer) with a X-ray source of Co-K α radiation ($\lambda = 1.7889 \text{ \AA}$) over a 2θ range of 20° to 80° at a scan step size of 0.05° . The X-ray tube voltage and current were fixed at 35 kV and 20 mA, respectively.

RESULTS

Figure 2 shows the epifluorescence microscopic image of the well grown MAB culture media in which the samples were exposed for the present study. The rod and cocci shaped bacteria are shown with markings in the figure. Figure 3 shows the epifluorescence microscopic image of the well grown SRB culture media.

Visualization of the Surfaces

The morphology of degradation in MAB and SRB cultures was evaluated by comparing with unexposed surfaces. Figure 4 shows the photographs of mortar specimens after exposure in MAB culture.

The attack over the surface of CC specimens appeared as blackening on the surface after exposure in both bacterial cultures. CF specimen surface showed white patches and presence of some segregates after exposure in MAB and SRB culture, respectively. The presence of white patchy layers was also observed over the surfaces of CFN specimens. However, no specific features were visible on the surfaces of CFNI specimens even after exposure to bacterial cultures.

Degradation Parameters in Microbial Cultures

The crushed pH of all the fresh mortar specimens was found to be above a value of 12. Table 2 shows the pH decrease on the surfaces of mortar specimens exposed to the MAB and SRB microbial cultures for a period of 7 days.

Among all the specimens, the pH reduction was found to be the least (11.98 and 11.94 for MAB and SRB cultures, respectively) for inhibitor admixed nanophase modified fly ash specimens (CFNI). CC specimens had comparatively larger reduction in pH values (11.61 and 11.53) after exposure in MAB and SRB culture, respectively. The reduction in pH values of CF and CFN specimens was between that of CC and CFNI specimens. The quantitative reduction in pH values after exposure in MAB/SRB cultures are also given in Table 2. CC specimens had a large reduction ($0.55 \pm 0.02/0.63 \pm 0.01$),

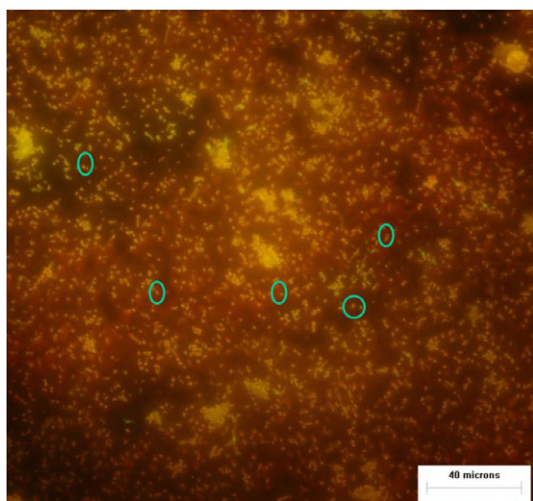


Figure 2. Epifluorescence image of grown MAB culture. [Color figure can be viewed at wileyonlinelibrary.com]

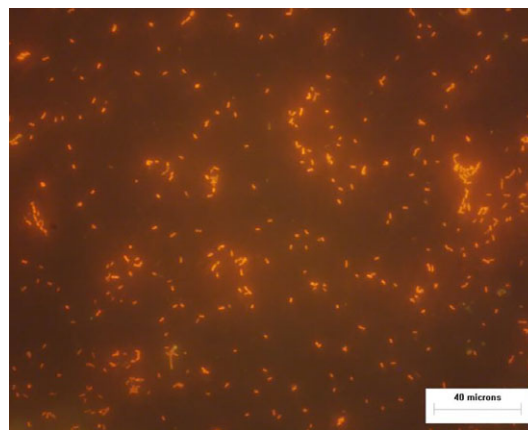


Figure 3. Epifluorescence image of grown SRB culture. [Color figure can be viewed at wileyonlinelibrary.com]

whereas CFNI specimens had the least reduction ($0.08 \pm 0.01/0.12 \pm 0.02$) in pH values after exposure to the microbial cultures.

Table 3 shows the reduction in thickness and diameter of specimens after 7 days of exposure in MAB culture. The reduction in thickness and diameter of CC specimens was found to be $0.47 \pm 0.04 \text{ mm}$ and $0.38 \pm 0.07 \text{ mm}$, respectively. However, CFNI specimens showed a reduction of $0.06 \pm 0.05 \text{ mm}$ and $0.05 \pm 0.08 \text{ mm}$ in thickness and diameter, respectively, after exposure in the culture. Further, the dimensional loss in CFN and CF specimens was found to be in between CC and CFNI specimens. Table 4 represents a comparison of the weight loss in different specimens. CC specimens and CF specimens showed more weight loss percentage indicating high levels of degradation (0.47% and 0.34%). CFNI specimens had the least weight loss (0.11%) among all the mixes.

Similarly, thickness and diameter of mortar specimens exposed to SRB culture were measured and compared with that of unexposed specimens and the corresponding reductions in both the parameters are tabulated in Table 3. The extent of degradation was found to be highest in case of CC specimens followed by CF specimens. The loss in thickness and diameter of CC specimens were found to be $0.43 \pm 0.04 \text{ mm}$ and $0.36 \pm 0.06 \text{ mm}$, respectively. However, CFNI specimens had a very minimal reduction in dimensional parameters after SRB attack. CFNI specimens exhibited a reduction of $0.06 \pm 0.04 \text{ mm}$ and $0.03 \pm 0.01 \text{ mm}$ in thickness and diameter, respectively. Both CFN and CF specimens showed the same trend as in the case of mixed bacterial culture.

Table 4 represents percentage weight loss of all the specimens. The control specimens showed the maximum weight loss (0.59%) and this could be due to high levels of degradation. However, the least reduction in weight was observed in the case of CFNI specimens (0.19%). CFN specimens also exhibited comparatively smaller reductions in weight (0.32%) compared with control specimens. CF specimens had more weight loss (0.51%) when compared with CFN and CFNI specimens.

Biofilm Characterization Studies in Bacterial Cultures

The density of bacterial film formed over the mortar specimens exposed in the MAB culture is represented in the form of TVC in Table 5. CC specimens showed the highest number of bacterial colonies ($6.43 \pm 0.3 \times 10^8 \text{ cfu/cm}^2$) when compared with other mixes. The lowest density of biofilm was found over the surface of CFNI specimens ($2.90 \pm 0.1 \times 10^4 \text{ cfu/cm}^2$). The CFN ($5.79 \pm 0.2 \times 10^5 \text{ cfu/cm}^2$) and CFNI

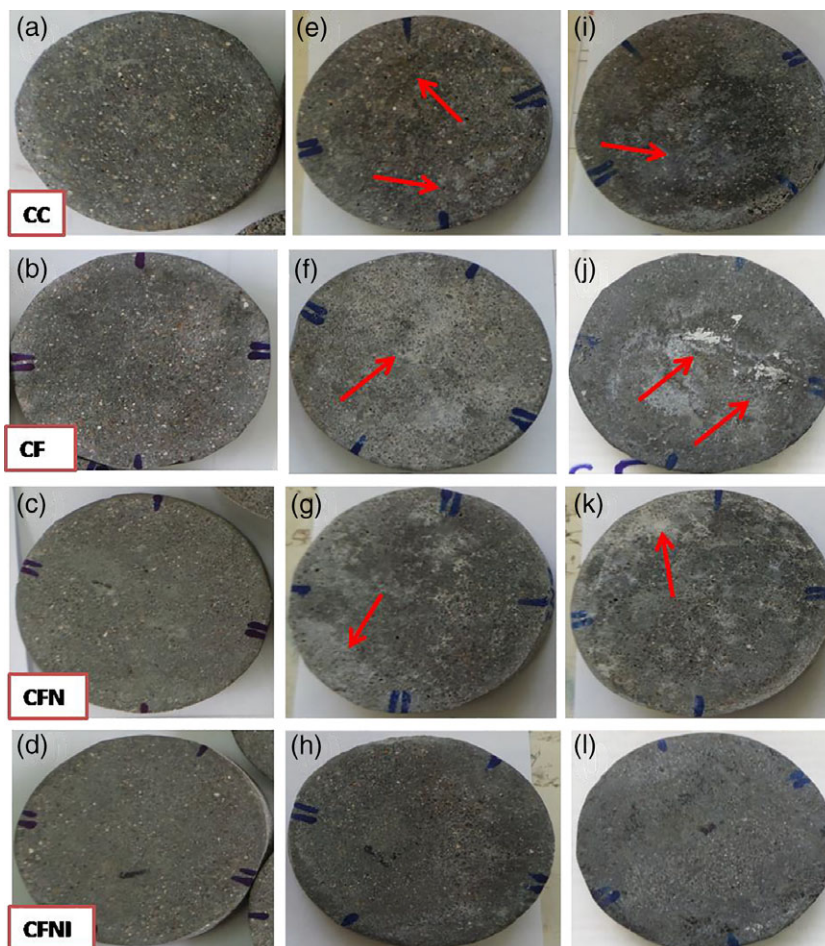


Figure 4. Specimens before and after exposure in MAB and SRB cultures. (a–d) Unexposed CC, CF, CFN, and CFNI specimens. (e–h) Specimens exposed in MAB culture. (i–l) Specimens exposed in SRB culture. [Color figure can be viewed at wileyonlinelibrary.com]

Table 2. pH of mortar specimens exposed in microbial cultures.

Type of specimen	Composition	pH before exposure	pH after exposure in bacterial culture MAB/SRB	Reduction in pH after exposure in MAB/SRB cultures
CC	100% OPC	12.16	11.61/11.53	$0.55 \pm 0.02/0.63 \pm 0.01$
CF	CC replaced with 40 wt % fly ash	12.02	11.78/11.72	$0.24 \pm 0.03/0.30 \pm 0.02$
CFN	CF replaced with 1 wt % TiO ₂ and 1 wt % CaCO ₃	12.04	11.92/11.90	$0.12 \pm 0.02/0.14 \pm 0.01$
CFNI	CFN replaced with 2 wt % NaNO ₂	12.06	11.98/11.94	$0.08 \pm 0.01/0.12 \pm 0.02$

specimens were observed to have three and four order reduction in the number of bacterial colonies, compared with CF and CC specimens, respectively. CF specimens had a one order reduction in the bacterial count ($1.67 \pm 0.2 \times 10^7$ cfu/cm²) compared with CC specimens.

The bacterial density over the surface of specimens exposed in SRB culture is shown in Table 5. Control specimens had the highest number of bacterial colonies over the surface ($3.86 \pm 0.4 \times 10^8$ cfu/cm²). CFNI ($7.72 \pm 0.1 \times 10^3$ cfu/cm²) specimens had a five order reduction in the bacterial count and CFN specimens ($2.09 \pm 0.2 \times 10^4$ cfu/cm²) had a four order reduction in the bacterial count. CF specimens showed a two order decrease in the number of bacterial colonies attached over the surface ($2.03 \pm 0.3 \times 10^6$ cfu/cm²).

Table 6 shown below gives the protein and carbohydrate content in biofilms after exposure in the MAB culture. The carbohydrate and protein content over CC specimens was 166.80

and 1.707 µg/cm², respectively. However, the biofilm formed over CFNI specimens showed the least organic content confirming the minimal biofilm formation over the surface. The carbohydrate and protein content over CFNI specimens was estimated to be 126.55 and 0.34 µg/cm², respectively. CFN specimens also showed comparatively reduced concentration of organic content whereas the biofilm attached over CF specimens had more carbohydrate and protein contents.

The amount of organic content present in the biofilm formed over the specimens exposed in SRB cultures are also tabulated in Table 6. The concentration of carbohydrate and protein over CC specimens were 167.32 and 12.06 µg/cm², respectively. CFNI specimens had much less organic content (84.62 µg/cm² of carbohydrate and 8.32 µg/cm² of protein) confirming least attachment on its surface. The organic content in CFN and CF specimens was between that of CFNI and CC specimens.

Table 3. Loss in dimensions after exposure in bacterial cultures.

Type of specimen	Loss in thickness (mm) MAB/SRB	Loss in diameter (mm) MAB/SRB
CC	0.47 ± 0.04/0.43 ± 0.04	0.38 ± 0.07/0.36 ± 0.06
CF	0.19 ± 0.06/0.17 ± 0.06	0.16 ± 0.07/0.16 ± 0.07
CFN	0.12 ± 0.06/0.10 ± 0.06	0.09 ± 0.02/0.08 ± 0.02
CFNI	0.06 ± 0.05/0.06 ± 0.04	0.05 ± 0.08/0.03 ± 0.01

Epifluorescence Microscopic Analysis

Epifluorescence micrographs of mortar specimens exposed in both MAB culture and SRB culture are shown in Figures 5 and 6, respectively. The micrographs showed that CC had more orange fluorescence indicating more actively metabolizing bacterial cells attached on the surface compared with modified mortar specimens in MAB culture [12]. Among all the specimens, CFNI showed least bacterial attachment, which was evident from the absence of orange fluorescence over the entire surface. The extent of bacterial attachment over the CFN surface was also not very high whereas CF surface had comparatively more bacterial attachment. A similar trend was observed in the case of specimens exposed in SRB culture.

Confocal Laser Scanning Microscopy Analysis

The surfaces of the specimens exposed in MAB were visualized under a CLSM and the 3D images of DAPI stained bacterial biofilms are given in Figure 7. The figure insets represents the orthographic images of the vertical cross sections (XZ) used to analyze the biofilm thickness. The biofilm thickness was highest on CC surface and least on CFNI surface. The thickness of biofilm over the specimens exposed in bacterial culture increased in the order of CFNI < CFN < CF < CC and are 12.65 ± 0.03 μm, 15.10 ± 0.02 μm, 18.12 ± 0.04 μm, and 38.25 ± 0.02 μm, respectively.

Figure 8 represents the 3D images of biofilms formed over the specimens in SRB culture. An increasing trend was also noticed in the thickness of biofilms formed over the surface in the order CFNI < CFN < CF < CC and are 0.1 ± 0.01 μm, 11.0 ± 0.02 μm, 20.0 ± 0.01 μm, and 45.0 ± 0.03 μm, respectively.

CLSM image analyses of various biofilm parameters with COMSTAT2 (Table 7) showed that the biofilm coverage area, diffusion distance, biomass, thickness distribution, and surface area was more on CC mortar specimens compared with modified mortar specimens in MAB culture. Area occupied by the biofilm on modified specimens is nearly 80%–90% less than that of control specimen after exposure in MAB culture. The biomass on the modified specimens has greatly reduced when compared with CC specimens. The diffusion distance calculated (the length of the shortest path from a voxel inside the biomass to the surface) indicated that biofilms on control specimens have more average diffusion distance than that on modified ones. The maximum biofilm thickness on the CC specimen (63.4075 μm) was higher than that of modified specimens among which CFNI showed the least thickness (36.0194 μm).

Table 4. Reduction in weight after exposure in bacterial cultures.

Type of specimen	Loss in weight (%) MAB	Loss in weight (%) SRB
CC	0.47 ± 0.02	0.59 ± 0.03
CF	0.34 ± 0.03	0.51 ± 0.02
CFN	0.26 ± 0.01	0.32 ± 0.01
CFNI	0.11 ± 0.01	0.19 ± 0.01

Table 5. Total Viability Count of specimens exposed in bacterial cultures.

Type of specimen	Total viable count (cfu/cm ²) MAB	Total viable count (cfu/cm ²) SRB
CC	6.43 ± 0.3 × 10 ⁸	3.86 ± 0.4 × 10 ⁸
CF	1.67 ± 0.2 × 10 ⁷	2.03 ± 0.3 × 10 ⁶
CFN	5.79 ± 0.2 × 10 ⁵	2.09 ± 0.2 × 10 ⁴
CFNI	2.90 ± 0.1 × 10 ⁴	7.72 ± 0.1 × 10 ³

The ratio of surface area to biovolume is lower on modified specimens than the CC specimen. The average thickness of the biomass over the CC specimen was found to be 29.50 μm and reduced to the order of 1.127 μm over CFNI specimen surface.

The detailed confocal image analysis of the various biofilm parameters on the specimens exposed in SRB culture is shown in Table 8. A similar trend was observed as in the case of specimens exposed in MAB culture. All the modified mortar specimens showed a reduction in all the parameters in comparison to CC mortar specimen. The maximum biofilm thickness was observed on the CC specimen (41.6332 μm), whereas CFNI specimen had the least biofilm thickness (22.2379 μm) among all the specimens.

XRD Analysis

Figure 9a shows the XRD pattern of CC specimens after exposure in both the cultures compared with unexposed specimens. Similarly, Figure 9b–d shows the XRD pattern of CF, CFN, and CFNI specimens exposed in microbial cultures compared with unexposed specimens. The Bragg diffraction peaks corresponding to silicon dioxide (SiO₂) is seen at 2θ values of 24.31°, 31.24°, 49.77°, and 58.96° (JCPDS 01-072-1088), calcium silicate hydrate (CSH) is seen at 2θ values of 21.10°, 32.54°, 34.33°, 39.93°, 46.20°, 55.4°, and 71.04° (JCPDS 00-029-0373) and calcium aluminium silicate (CAS) at 2θ value of 57.65° and 59.1° (JCPDS 01-083-1278). However, the SiO₂ peak was most intense on CC specimen due to the high cement content available per unit volume. This intensity decreased on all the other three specimens due to the replacement of cement content. However, CFNI specimens had an intense SiO₂ peak as compared with CF and CFN specimens.

The number of peaks observed was more for the specimens exposed to the microbial cultures as compared with unexposed specimens. However, the intensity of SiO₂ peaks got drastically reduced on CC and CF specimens, whereas, the intensity of SiO₂ peak still got retained on CFN, and CFNI specimens. The peaks corresponding to calcium carbonate was observed at 2θ values of 25.62° on CF, CFN, and CFNI specimens (JCPDS 00-041-1475) and at 42.69°, 50.3°, and 53.79° on CC and CF specimens (JCPDS 00-029-0305) after exposure in MAB culture. But, the high intensity peak of calcium carbonate was observed at 50.3° only in CC specimens.

After exposure in SRB culture, the intensity of SiO₂ and CSH got drastically reduced in CC and CF specimens. However, intensity reduction was least on CFN and CFNI specimens. The peaks corresponding to calcium aluminum sulfate

Table 6. Biochemical compositions of biofilms formed over specimens exposed in bacterial cultures.

Type of specimens	Concentration of carbohydrate (μg/cm ²) MAB/SRB	Concentration of protein (μg/cm ²) MAB/SRB
CC	166.80/167.32	1.707/12.06
CF	162.43/122.05	0.88/11.30
CFN	144.29/99.28	0.54/8.94
CFNI	126.55/84.62	0.34/8.32

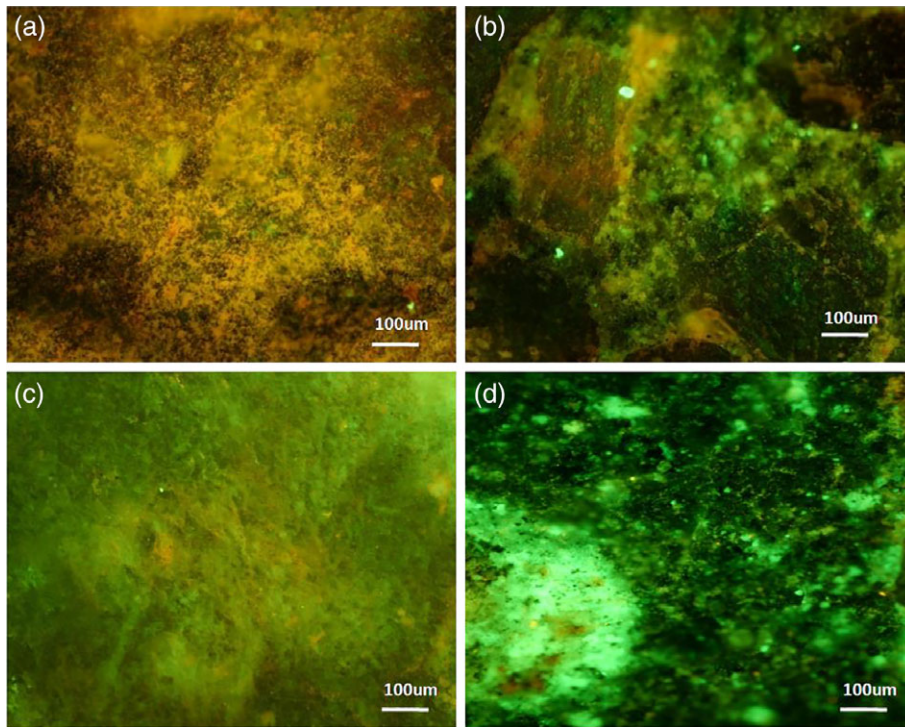


Figure 5. Epifluorescence micrographs of mortar specimens exposed in MAB culture. (a) CC, (b) CF, (c) CFN, and (d) CFNI. [Color figure can be viewed at wileyonlinelibrary.com]

hydroxide hydrate (ettringite) were observed at 2θ values of 28.27° , 47.30° , 49.15° , and 57.4° on CC and CF specimens, 60.32° and 73.81° on CF specimens and 47.30° and 57.4° on CFN specimens (JCPDS 00-041-1451). But, no peak of ettringite was observed for CFNI specimen.

DISCUSSION

Fresh concrete is highly alkaline in nature with a pH range of 11–13. Therefore, microbes generally do not attach to the surface of a fresh concrete. However, the highly permeable concrete skin allows the penetration of different ions in

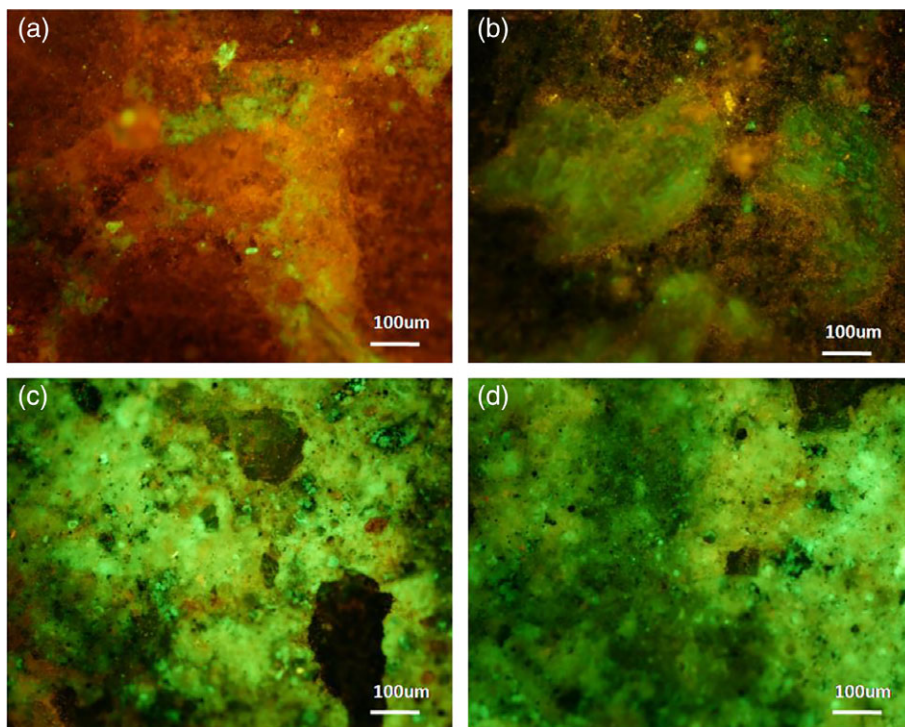


Figure 6. Epifluorescence micrographs of mortar specimens exposed in SRB culture. (a) CC, (b) CF, (c) CFN, and (d) CFNI. [Color figure can be viewed at wileyonlinelibrary.com]

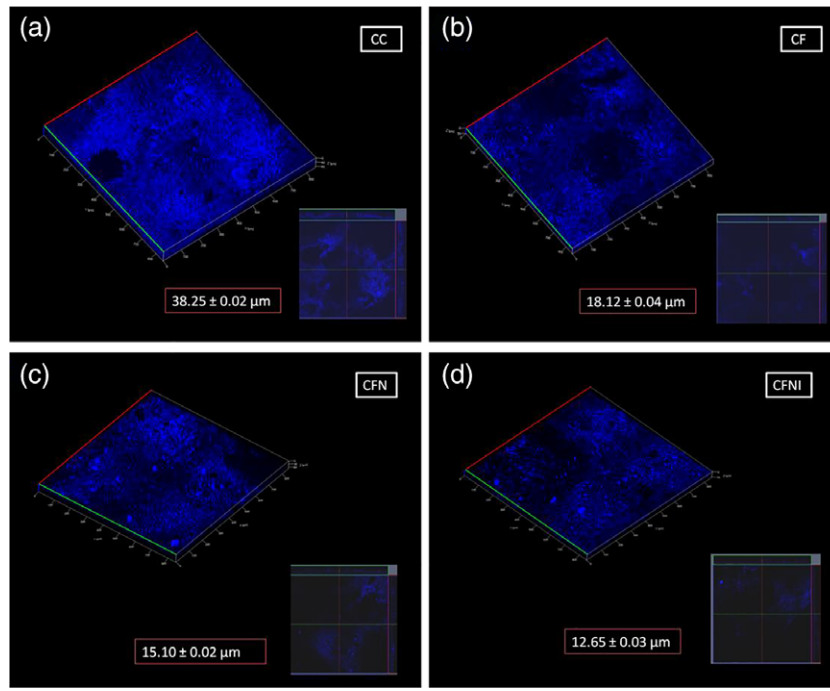


Figure 7. Confocal microscopic images of mortar specimens exposed in MAB culture. (a) CC, (b) CF, (c) CFN, and (d) CFNI. [Color figure can be viewed at wileyonlinelibrary.com]

atmosphere and seawater, leading to a decrease in pH [37,38]. Once the pH is lowered, heterotrophic bacteria and fungus colonize concrete surfaces and lead to biodeterioration [2]. Various efforts are made to improve the density of the concrete matrix with an impermeable skin by incorporation of Supporting Information Materials. Studies conducted by Vinita *et al.* [4] has shown that the pH of concrete specimens incorporated with fly ash was high even after exposure to microbial

cultures in comparison to control concrete. Sudha *et al.* [15] has carried out studies on nanophase modified fly ash concrete and reported that pH was higher for concrete integrated with nanoparticles than for fly ash concrete after exposure in seawater. Many investigators have shown that addition of TiO₂ nanoparticles can retard pH degradation [13,14]. In this study, comparison of four types of mortars clearly showed that through combined incorporation of fly ash, nanoparticles, and

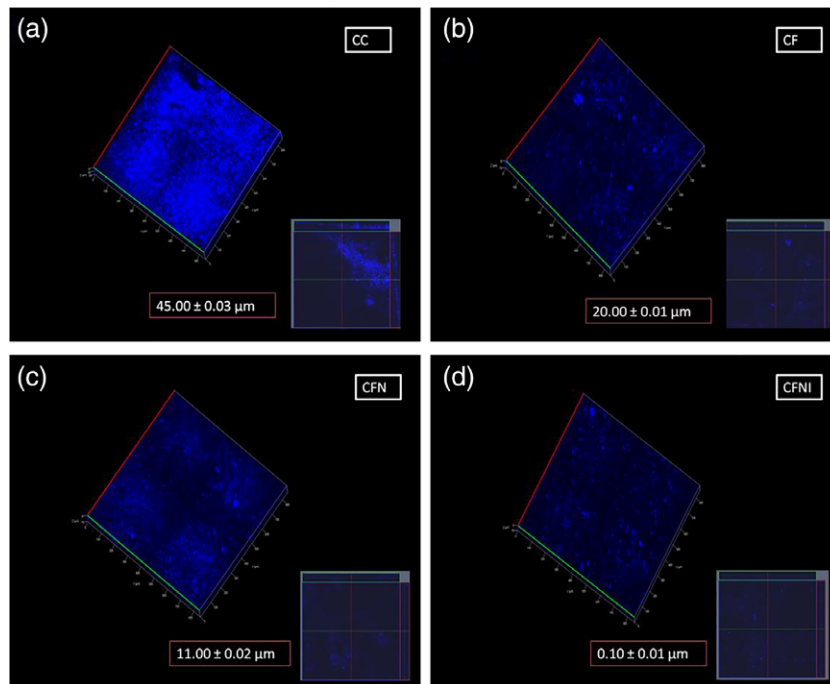


Figure 8. Confocal microscopic images of mortar specimens exposed in SRB culture. (a) CC, (b) CF, (c) CFN, and (d) CFNI. [Color figure can be viewed at wileyonlinelibrary.com]

Table 7. COMSTAT analyses on confocal images of mortar specimens exposed to MAB culture.

Type of specimen	Area occupied (μm^2)	Biomass ($\mu\text{m}^3/\mu\text{m}^2$)	Diffusion distance (μm) (ave. diff. dist in μm)	Maximum thickness (μm)	Surface area to biovolume ratio ($\mu\text{m}^2/\mu\text{m}^3$)	Average thickness (biomass) (μm)
CC	25,296.07	1.10706	14.34284 (0.01777)	63.4075	5.75726	29.50203
CF	2110.76	0.10828	10.21954 (0.00104)	56.004	3.22073	28.79626
CFN	1229.1	0.02921	9.32828 (0.00267)	53.3428	2.24544	18.815
CFNI	414.98	0.00296	8.62343 (0.00003)	36.0194	0.72554	1.12724

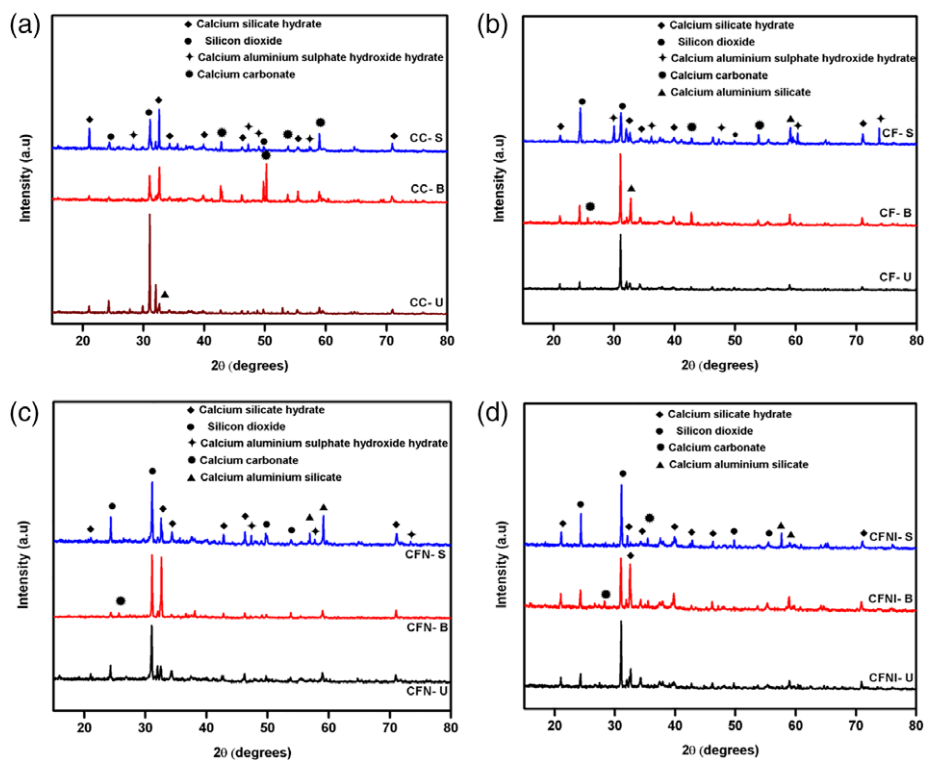
Table 8. COMSTAT analyses on confocal images of mortar specimens exposed to SRB culture.

Type of specimen	Area occupied (μm^2)	Biomass ($\mu\text{m}^3/\mu\text{m}^2$)	Diffusion distance (μm) (ave. diff. dist in μm)	Maximum thickness (μm)	Surface area to biovolume ratio ($\mu\text{m}^2/\mu\text{m}^3$)	Average thickness (biomass) (μm)
CC	12,421.16	1.76379	15.24953 (0.05107)	78.2345	2.69523	41.6332
CF	1047.63	0.11015	13.9253 (0.0468)	75.5698	2.10047	34.48764
CFN	905.11	0.09795	13.8008 (0.01702)	58.4589	1.68023	32.06338
CFNI	375.54	0.013651	13.31596 (0.00464)	51.2414	1.6406	22.2379

inhibitor, the decrease in pH was slowed down further. A one order decrease in the pH reduction was observed on CFNI compared with CC (Table 2).

This slow reduction in pH is seen to have an effect on the bacterial adhesion and biofilm formation. The bacterial density, viability, and biofilm thickness in both aerobic and anaerobic culture media was found to be highest on CC and lowest on CFNI among the four types of concrete mortar specimens

(Table 5). Addition of TiO_2 nanoparticles with its photocatalytic activity is shown to have antibacterial activity due to the formation of free radicals that can oxidize organic biomass [39–41]. Sudha *et al.* [15] has shown a one order decrease in the viable bacterial count on incorporation of TiO_2 nanoparticles. In the present study, a four order decrease in aerobic bacterial density and five order decrease in the SRB density were shown by the CFNI mix. There was also an enhancement

**Figure 9.** XRD pattern of specimens exposed in bacterial cultures (a) CC unexposed, CC exposed to MAB and SRB cultures. (b) CF unexposed, CF exposed to MAB and SRB cultures. (c) CFN unexposed, CFN exposed to MAB and SRB cultures. (d) CFNI unexposed, CFNI exposed to MAB and SRB cultures. [Color figure can be viewed at wileyonlinelibrary.com]

observed with each additive. Fly ash addition showed a two order decrease, whereas fly ash with nanoparticles showed a three order decrease. Finally when inhibitor is added with fly ash and nanoparticles, a four to five order decrease was observed due to the synergy among all the additives. The bactericidal activity of sodium nitrite on most of the bacterial species has been reported by Klebanoff *et al.* [42] and Stanojevic *et al.* [43]. They reported that sodium nitrite *in vivo* conditions form a toxic intermediate in amino acid metabolism and thus, exhibit the bactericidal properties. Quantitative analysis of biofilm biomass as protein and carbohydrates also confirmed maximum reduction on CFNI surface as compared with all other types of mortar specimens (Table 6).

George *et al.* [44] has shown that the reduction in dimensional parameters is indicative of the extent of biodegradation in the specimens. In this study, visual imaging showed no evidence of post exposure changes in the morphology on the surface of CFNI specimens (Figure 4). The weight loss and dimensional changes were also quantified. CC specimens showed the maximum degradation whereas negligible reduction in the dimensional parameters is observed in the case of CFNI and CFN specimens after exposure in both the cultures (Table 3). CFNI specimens had the least degree of weight loss among all the mixes (Table 4). The extent of biofilm formation was lowest over CFNI specimens in both the cultures, as evident from the epifluorescence micrographs (Figures 5 and 6). This was further corroborated by the confocal microscopy images which showed the lowest biofilm thickness over CFNI specimens (Figures 7 and 8). The COMSTAT analysis of the confocal images was well in agreement with the quantified results (Tables 7 and 8). In addition to the antibacterial activity, nanoparticles also act as fillers [45] whereas, nitrite ions are reported to have good antimicrobial activity [46,47], thereby increasing the degradation resistance of CFNI specimens.

XRD pattern further showed the mineralogical changes in the mortar specimens under the biofilm formation. Literature shows that formation of calcium carbonate in concrete reduce the interstitial pH and leads to degradation [48,49]. XRD pattern shows evolution of new calcium carbonate peaks (at 2 θ positions of 25.62°, 42.69°, 50.3°, and 53.79°) after exposure in MAB culture (Figure 9). These peaks were observed to be more on CC and CF mortar specimens. CC specimens showed a high intense peak of calcium carbonate at 50.3°, whereas the intensity was less on other specimens. It has been reported that under the biochemical activities of bacteria due to lowering of pH, calcium carbonate will be formed, which is termed as the process of carbonation [50]. During the metabolism of bacterial species, it releases CO₂ that reacts with (Ca²⁺) resulting in the precipitation of minerals [51] and decreases the alkalinity [52,53]. The intensity of calcium carbonate peaks was found to be less on CFNI and CFN specimens due to the resistance of these concrete mortar mixes against carbonation in the presence of nanoparticles and inhibitor. Further, the crystallite size of SiO₂, calculated using Scherrer formulae showed that the crystallite size of SiO₂ got reduced after exposure in both the cultures for all the specimen types. However, the least reduction in crystallite size was observed for CFNI and CFN specimens, which may be due to the less bacterial density on these specimens.

The mortar specimens exposed to SRB culture medium showed the presence of another deterioration phase (ettringite). The biogenic sulfuric acid produced due to the action of sulfate reducing bacteria, reacts with free lime from the concrete and forms gypsum [54]. The formation of more gypsum on the concrete surfaces leads to the formation of ettringite that can initiate the cracking of the concrete [55,56]. More ettringite peaks with high intensity were observed on CC, CF, and CFN specimens as compared with CFNI specimen.

Thus, from the short term exposure studies, it can be concluded that in aggressive aerobic and anaerobic bacterial

culture the mortar specimens incorporated with 40 wt % fly ash, 2 wt % nanoparticles (1 wt % TiO₂ and 1 wt % CaCO₃), and 2 wt % sodium nitrite inhibitor exhibited excellent antibacterial activity as shown by the reduced amount of bacterial growth (Table 5), and resistance to biodegradation as shown by the small amount of weight and thickness loss (Tables 3 and 4) due to the synergistic effects of supplements.

CONCLUSIONS

From the anti-bacterial studies on four different types of mortar specimens namely CC, CF, CFN, and CFNI, after a week-long exposure in aerobic and anaerobic bacterial culture, the following conclusions were made. A negligible decrease in the pH of CFNI mortar specimens was observed as compared with CC (0.08 in CFNI against 0.55 in CC). The loss in thickness, diameter, and weight were the lowest on CFNI mortar specimens. The total bacterial density reduction observed in CF, CFN, and CFNI mortar specimen surfaces exposed to bacterial cultures were two, three, and five orders of magnitude, respectively, as compared with CC specimens. The biochemical constituents were also lowest on CFNI mortar specimen surfaces among the three types of specimens.

Epifluorescence micrographs confirmed complete absence of orange fluorescence of viable bacterial cells on CFNI specimens. Biofilm thickness estimated from the 3D CLSM images was also the lowest on CFNI specimen surfaces. XRD spectra revealed the smallest number of CaCO₃ peaks after exposure in MAB culture and sulfate peaks after exposure in SRB culture on the surface of CFNI specimens. The experimental results indicated a progressive increase in antibacterial activity and biodegradation resistance in the order of CC < CF < CFN < CFNI, confirming the synergistic effect of fly ash, nanoparticles and inhibitor in CFNI specimens.

ACKNOWLEDGMENTS

The authors would like to thank Mr. Rathish. V.R and Dr. M.S. Haji Sheik Mohammed, Department of civil engineering, B.S. Abdur Rahman Crescent Institute of Science and Technology, Chennai for providing extended help for casting the concrete specimens. The authors sincerely acknowledge Director, IGCAR for his constant encouragement throughout this study. The fellowship provided by DAE, Govt. of India for carrying out this research is also acknowledged.

LITERATURE CITED

1. Yamanaka, T., Aso, I., Togashi, S., Tanigawa, M., Shoji, K., Watanabe, T., Watanabe, N., Maki, K., & Suzuki, H. (2002). Corrosion by bacteria of concrete in sewerage systems and inhibitory effects of formates on their growth, *Water Research*, 36, 2636–2642.
2. Ramachandran, D., George, R.P., Vishwakarma, V., & Kamachi Mudali, U. (2017). Strength and durability studies of fly ash concrete in sea water environments compared with normal and superplasticizer concrete, *KSCE Journal of Civil Engineering*, 21, 1282–1290.
3. George, R.P., Vishwakarma, V., Samal, S.S., & Kamachi Mudali, U. (2012). Current understanding and future approaches for controlling microbially influenced concrete corrosion: a review, *Concrete Research Letters*, 3, 491–506.
4. Vishwakarma, V., George, R.P., Ramachandran, D., Anandkumar, B., & Kamachi Mudali, U. (2013). Studies of detailed Biofilm characterization on fly ash concrete in comparison with normal and superplasticizer concrete in seawater environments, *Environmental Technology*, 35, 42–51.
5. Rose, A.H. (1981). *Microbe biodeterioration economic microbiology*. (Volume 6, pp. 35–80), London: Academic Press.
6. Vigneron, A., Head, I.M., & Tsesmetzis, N. (2018). Damage to offshore production facilities by corrosive microbial

- biofilms, *Applied Microbiology and Biotechnology*, 102, 2525–2533.
7. Cwalina, B. (2008). Biodeterioration of concrete, *Architecture, Civil Engineering, Environment*, 4, 133–140.
 8. Silva, M.R. & Nail, T.R., (2013). Biodeterioration of concrete structures in coastal zone. In *Proceeding of III international conference on sustainable construction materials and technologies*, Kyoto.
 9. Yasantha Abeyesundara, U.G., & Babel, S. (2010). A quest for sustainable materials for building elements in Sri Lanka Foundations, *Environmental Progress & Sustainable Energy*, 29, 370–381.
 10. Kim, R.H., Tae, S.H., Yang, K.H., Kim, T.H., & Roh, S.J. (2015). Analysis of lifecycle CO₂ reduction performance for long-life apartment house, *Environmental Progress & Sustainable Energy*, 34, 555–566.
 11. Cho, M.S., & Noh, J.M. (2012). Assessment of properties and durability of fly ash concrete used in Korean nuclear power plants, *Nuclear Engineering and Technology*, 44, 331–342.
 12. Shaikh, F.U., & Supit, S.W. (2014). Mechanical and durability properties of high volume fly ash (HVFA) concrete containing calcium carbonate (CaCO₃) nanoparticles, *Construction and Building Materials*, 70, 309–321.
 13. Nazari, A., Sh, R., Sh, R., Shamekhi, S.F., & Khademno, A. (2010). Assessment of the effects of the cement paste composite in presence of TiO₂ nanoparticles, *Journal of American Science*, 6, 43–46.
 14. Vishwakarma, V., Sudha, U., Ramachandran, D., Anandkumar, B., George, R.P., Kumari, K., Preetha, R., Mudali, U.K., & Pillai, C.S. (2016). Enhancing antimicrobial properties of fly ash mortars specimens through nanophase modification, *Materials Today: Proceedings*, 3, 1389–1397.
 15. Uthaman, S., George, R.P., Vishwakarma, V., Ramachandran, D., Thinaharan, C., Viswanathan, K., & Mudali, U.K. (2018). Surface modification of fly ash concrete through nanophase incorporation for enhanced chemical deterioration resistance, *Journal of Bio- and Tribo-Corrosion*, 4, 15.
 16. Montes-Garcia, P., Jiménez-Quero, V., & López-Calvo, H. (2015). Assessment of high performance concrete containing fly ash and calcium nitrite based corrosion inhibitor as a mean to prevent the corrosion of reinforcing steel, *Journal of Physics: Conference Series*, 582, 012028.
 17. Ormellese, M., Berra, M., Bolzoni, F., & Pastore, T. (2006). Corrosion inhibitors for chlorides induced corrosion in reinforced concrete structures, *Cement and Concrete Research*, 36, 536–547.
 18. Kim, K.T., Kim, H.W., Chang, H.Y., Lim, B.T., Park, H. B., & Kim, Y.S. (2015). Corrosion inhibiting mechanism of nitrite ion on the passivation of carbon steel and ductile cast iron for nuclear power plants, *Advances in Materials Science and Engineering*, 2015, 1–16.
 19. Montes, P., Bremner, T.W., & Lister, D.H. (2004). Influence of calcium nitrite inhibitor and crack width on corrosion of steel in high performance concrete subjected to a simulated marine environment, *Cement and Concrete Composites*, 26, 243–253.
 20. ASTM C494 (2004). *Standard Specification for chemical admixtures for concrete*, Philadelphia: American Society for Testing and Materials.
 21. Epanand, R.M., & Vogel, H.J. (1999). Diversity of antimicrobial peptides and their mechanisms of action, *Biochimica et Biophysica Acta (BBA) – Biomembranes*, 1462, 11–28.
 22. Postgate, J.R. (1984). *The sulphate reducing bacteria*. (2nd Edition, pp. 38–45), Cambridge, UK: Cambridge University Press.
 23. APHA (1989). *Standard methods for the examination of water and waste water*. (14th Edition), Washington, DC: APHA.
 24. Ohemeng-Ntiamoah, J., & Datta, T. (2018). Evaluating analytical methods for the characterization of lipids, proteins and carbohydrates in organic substrates for anaerobic co-digestion, *Bioresource Technology*, 247, 697–704.
 25. Dubois, M., Gilles, K.A., Hamilton, J.K., Rebers, P.T., & Smith, F. (1956). Colorimetric method for determination of sugars and related substances, *Analytical Chemistry*, 28, 350–356.
 26. Lowry, O.H., Rosebrough, N.J., Farr, A.L., & Randall, R.J. (1951). Protein estimation by Lowry's method, *Journal of Biological Chemistry*, 193, 265.
 27. Darzynkiewicz, Z. (1990). Differential staining of DNA and RNA in intact cells and isolated cell nuclei with acridine orange, *Methods in Cell Biology*, 33, 285–298.
 28. Mah, T.F.C., & O'Toole, G.A. (2001). Mechanisms of biofilm resistance to antimicrobial agents, *Trends in Microbiology*, 9, 34–39.
 29. Ratinen, H. (1972). X-ray-excited optical fluorescence from pure and rare-earth-doped magnesium and calcium oxides, *Physica Status Solidi (a)*, 12, 175–180.
 30. Lawrence, J.R., & Neu, T.R. (1999). Confocal laser scanning microscopy for analysis of microbial biofilms, *Methods in Enzymology*, 310, 131–144.
 31. Krawczyk-Bärsch, E., Grossmann, K., Arnold, T., Hofmann, S., & Wobus, A. (2008). Influence of uranium (VI) on the metabolic activity of stable multispecies biofilms studied by oxygen microsensors and fluorescence microscopy, *Geochimica et Cosmochimica Acta*, 72, 5251–5265.
 32. Rodriguez, G.G., Phipps, D., Ishiguro, K., & Ridgway, H.F. (1992). Use of fluorescent redox probe for direct visualization of actively respiring bacteria, *Applied and Environmental Microbiology*, 58, 1801–1808.
 33. Jiang, W., Xia, S., Duan, L., & Hermanowicz, S.W. (2015). Biofilm architecture in a novel pressurized biofilm reactor, *Biofouling*, 31, 321–331.
 34. Kurtis, K.E., El-Ashkar, N.H., Collins, C.L., & Naik, N.N. (2003). Examining cement-based materials by laser scanning confocal microscopy, *Cement and Concrete Composites*, 25, 695–701.
 35. Heydorn, A., Nielsen, A.T., Hentzer, M., Sternberg, C., Givskov, M., Ersboll, B.K., & Molin, S. (2000). Quantification of biofilm structures by the novel computer program COMSTAT, *Microbiology*, 146, 2395–2407.
 36. Singhal, D., Boase, S., Field, J., Jardeleza, C., Foreman, A., & Wormald, P.J. (2012). Quantitative analysis of in vivo mucosal bacterial biofilms, *International Forum of Allergy & Rhinology*, 2, 57–62.
 37. Uthaman, S., Vishwakarma, V., George, R.P., Ramachandran, D., Kumari, K., Preetha, R., Premila, M., Rajaraman, R., & Mudali, U.K. (2018). Enhancement of strength and durability of fly ash concrete in seawater environments: synergistic effect of nanoparticles, *Construction and Building Materials*, 187, 448–459.
 38. Lea, F.M. (1970). *The chemistry of cement and concrete*. (3rd Edition), London, UK: Edward Arnold Ltd.
 39. Chong, M.N., Jin, B., Chow, C.W., & Saint, C. (2010). Recent developments in photocatalytic water treatment technology: a review, *Water Research*, 44, 2997–3027.
 40. Foster, H.A., Ditta, I.B., Varghese, S., & Steele, A. (2011). Photocatalytic disinfection using titanium dioxide: spectrum and mechanism of antimicrobial activity, *Applied Microbiology and Biotechnology*, 90, 1847–1868.
 41. Sunada, K., Watanabe, T., & Hashimoto, K. (2003). Studies on photo killing of bacteria on TiO₂ thin film, *Journal of Photochemistry and Photobiology A: Chemistry*, 156, 227–233.
 42. Klebanoff, S.J. (1993). Reactive nitrogen intermediates and antimicrobial activity: role of nitrite, *Free Radical Biology and Medicine*, 14, 351–360.
 43. Stanojevic, D., Comic, L., Stefanovic, O., & Solujic-Sukdolac, S. (2009). Antimicrobial effects of sodium

- benzoate, sodium nitrite and potassium sorbate and their synergistic action in vitro, *Bulgarian Journal of Agricultural Science*, 15, 307–311.
44. George, R.P., Ramya, S., Ramachandran, D., & Mudali, U. K. (2013). Studies on biodegradation of normal concrete surfaces by fungus *Fusarium* sp, *Cement and Concrete Research*, 47, 8–13.
 45. Bastos, G., Patiño-Barbeito, F., Patiño-Cambeiro, F., & Armesto, J. (2016). Admixtures in cement-matrix composites for mechanical reinforcement, sustainability and smart features, *Materials*, 9, 972.
 46. Yarbrough, J.M., Rake, J.B., & Eagon, R.G. (1980). Bacterial inhibitory effects of nitrite: inhibition of active transport, but not of group translocation, and of intracellular enzymes, *Applied and Environmental Microbiology*, 39, 831–834.
 47. Buchanan, R.L., Stahl, H.G., & Whiting, R.C. (1989). Effects and interactions of temperature, pH, atmosphere, sodium chloride, and sodium nitrite on the growth of *Listeria monocytogenes*, *Journal of Food Protection*, 52, 844–851.
 48. Villain, G., Thiery, M., & Platret, G. (2007). Measurement methods of carbonation profiles in concrete: thermogravimetry, chemical analysis and gammadensimetry, *Cement and Concrete Research*, 37, 1182–1192.
 49. Papadakis, V.G., Vayenas, C.G., & Fardis, M.N. (1991). Physical and chemical characteristics affecting the durability of concrete, *ACI Materials Journal*, 8, 186–196.
 50. Garrett, T.R., Bhakoo, M., & Zhang, Z. (2008). Bacterial adhesion and biofilms on surfaces, *Progress in Natural Science*, 18, 1049–1056.
 51. Benzerara, K., Miot, J., Morin, G., Ona-Nguema, G., Skouri-Panet, F., & Ferard, C. (2011). Significance, mechanisms and environmental implications of microbial biomineralization, *Comptes Rendus Geoscience*, 343, 160–167.
 52. Smith, G.K. (2016). Calcite straw stalactites growing from concrete structures, *Cave & Karst Science*, 43, 4–10.
 53. Roberts, D.J., Nica, D., Zuo, G., & Davis, J.L. (2002). Quantifying microbially induced deterioration of concrete: initial studies, *International Biodeterioration & Biodegradation*, 49, 227–234.
 54. Attiogbe, E.K., & Rizkalla, S.H. (1988). Response of concrete to sulphuric acid attack, *ACI Materials Journal*, 17, 481–488.
 55. Noeiaghahi, T., Mukherjee, A., Dhami, N., & Chae, S.R. (2017). Biogenic deterioration of concrete and its mitigation technologies, *Construction and Building Materials*, 149, 575–586.
 56. Rahman, M.A., Halfar, J., & Shinjo, R. (2013). X-ray diffraction is a promising tool to characterize coral skeletons, *Advances in Materials Physics and Chemistry*, 3, 120–125.
-